Structure of DNA-CTAB-hexanol complexes

Rema Krishnaswamy,[1] Georg Pabst,[2] Michael Rappolt,[2] V. A. Raghunathan,[1] and A. K. Sood[3]
[1]*Raman Research Institute, Bangalore 560 080, India*
[2]*Institute of Biophysics and X-Ray Structure Research, Austrian Academy of Sciences, Schmiedlstraße 6, 8042 Graz, Austria*
[3]*Department of Physics, Indian Institute of Science, Bangalore 560 012, India*
(Received 14 September 2005; published 3 March 2006)

We have probed structures of the complexes formed by DNA with the cationic surfactant cetyltrimethylammonium bromide in the presence of the cosurfactant hexanol, using small angle x-ray diffraction techniques. They are found to exhibit a hexagonal→lamellar→hexagonal transition with increasing hexanol content. Quantitative analysis of the diffraction data shows that the complexes formed at low hexanol concentrations have an intercalated hexagonal (H_I) structure, whereas those formed at higher hexanol content have an inverted hexagonal (H_{II}) structure.

DOI: 10.1103/PhysRevE.73.031904 PACS number(s): 87.15.By, 61.30.Eb, 61.10.Eq

I. INTRODUCTION

DNA is known to form complexes with oppositely charged lipids and surfactants in aqueous solutions, which are of interest due to their fascinating electrostatics and their potential for biomedical applications [1–4]. The entropy gained by the release of counterions that are initially condensed on the DNA as well as on the surfactant aggregates drives this complexation [5–7]. These complexes exhibit charge inversion, which has been explained in terms of lateral correlation between the polyion chains [8]. X-ray diffraction studies have shown that complexes of DNA with double-tailed cationic lipids form an intercalated lamellar phase, which consists of DNA strands sandwiched between the lipid bilayers [Fig. 1(a)]. The DNA strands in the plane of the bilayers form a two-dimensional smectic with no positional correlations across the bilayers [9]. With the addition of neutral lipids that have a negative spontaneous curvature, or in the presence of cosurfactants such as hexanol, two-dimensional hexagonal structures are formed by these complexes [2]. The values of their lattice parameter are consistent with the inverted hexagonal structure H_{II}, where the lipid-coated DNA strands are arranged on a two-dimensional hexagonal lattice [Fig. 1(b)]. However, no detailed analysis of the diffraction data has been reported until now that confirms such a structure.

A two-dimensional (2D) intercalated hexagonal structure (H_I) has also been proposed for complexes of DNA with the single-tailed cationic surfactant cetyltrimethylammonium bromide (CTAB), consisting of DNA strands surrounded by three cylindrical micelles [Fig. 1(c)] [4,10]. The addition of a cosurfactant, such as hexanol, to a CTAB solution is known to decrease the spontaneous curvature of the surfactant aggregates, transforming them from cylinders to bilayers [11]. Further, short chain alcohols also substantially lower the bending rigidity of bilayers [12]. Hence cosurfactants can significantly modify the structure of these complexes. We have recently reported reentrant phase transitions driven by DNA and hexanol concentrations in CTAB-DNA-hexanol complexes, and the formation of two hexagonal structures [13]. The diffraction pattern of the hexagonal structure found at low hexanol content is very similar to that of the H_I structure observed in the absence of hexanol. Therefore, it was identified as H_I [Fig. 1(c)], whereas the hexagonal structure observed at high hexanol content was tentatively identified as inverted hexagonal (H_{II}) [Fig. 1(c)], similar to that proposed in some lipid-DNA complexes [2]. A partial phase diagram of this system, showing the different structures of the complexes obtained on varying the DNA and hexanol concentrations, has been given in Ref. [13], where the possible origins of the various phase transitions are also discussed. In order to characterize these structures more thoroughly, we have carried out higher resolution small angle x-ray diffraction experiments using a synchrotron beamline. The diffraction patterns of the different structures obtained from these experiments are consistent with those presented in Ref. [13], which were obtained using a laboratory source. In this paper we also present a detailed analysis of the diffraction data from these complexes, which substantiates the two hexagonal structures proposed by us earlier [13].

II. EXPERIMENTAL SECTION

CTAB (purity >99%) and hexanol were purchased from Aldrich. Sodium salt of highly polymerized calf thymus DNA was obtained from Sigma. All chemicals were used as received without further purification. CTAB-hexanol solutions with the hexanol to CTAB molar ratio (β =[hexanol]/[CTAB]) varying from 0 to 10 were first prepared in deionized water (Millipore), with the CTAB concentration fixed at 10 mM. DNA was then added to the surfactant solution to achieve the required relative concentration Γ=(wt. of CTAB)/(wt. of DNA). Samples were made with DNA concentration varying over a wide range about the isoelectric point (Γ_{iso}=1.1), where the total charge on the DNA strands is balanced by that on the CTA^+ ions. The complexes, which form immediately, were allowed to equilibrate for about a week and later transferred into a 1 mm diameter glass capillary (Mark) along with some of the supernatant for x-ray diffraction studies. The supernatant is a very dilute solution of either DNA or CTAB, depending on their relative concentration, and hence does not contribute to the intensi-

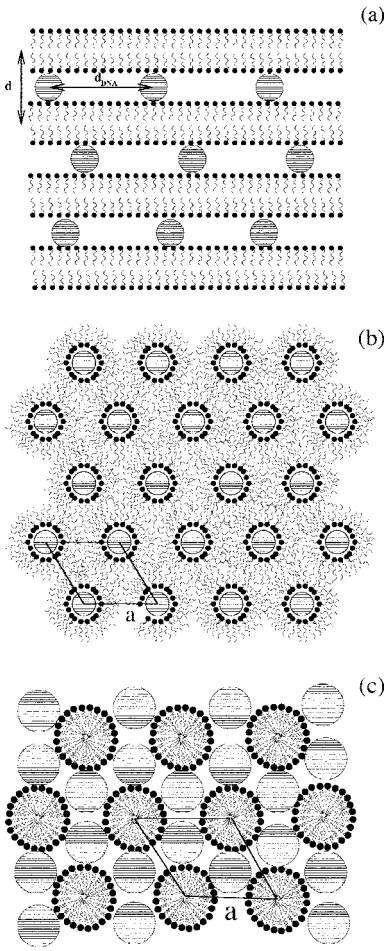

FIG. 1. Schematic of (a) the lamellar structure of DNA-lipid complexes, where the DNA strands, represented by the filled circles, are sandwiched between the lipid bilayers; (b) the inverted hexagonal (H_{II}) structure, where the lipid-covered DNA strands are packed in a two-dimensional hexagonal lattice; and (c) the intercalated hexagonal (H_I) structure, where each DNA strand is surrounded by three cylindrical micelles. Note that each unit cell in (b) contains one DNA strand surrounded by an inverted cylindrical micelle, whereas in (c) it contains one cylindrical micelle and two DNA strands.

ties of the diffraction peaks from the complex. The experiments were carried out at the Austrian SAXS beamline [14] at the Elettra synchrotron source, Trieste, Italy. The wavelength of x-rays used was 0.155 nm and the typical instrumental resolution [full width at half maximum (FWHM)] was $\delta q \sim 2.2 \times 10^{-2}$ nm. X-ray diffraction patterns were recorded using a one-dimensional position sensitive gas detector and were corrected for background scattering.

III. RESULTS AND DISCUSSION

All complexes obtained are found to be birefringent under a polarizing microscope. At low hexanol concentrations ($\beta < 5.0$) x-ray diffraction patterns consist of three peaks in the small angle region with their scattering vector q in the ratio $1:\sqrt{(3)}:2$. Diffraction patterns over this range of β are very

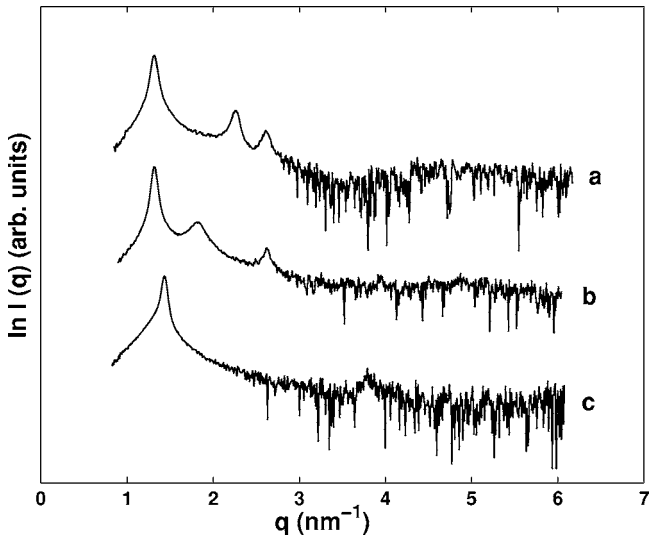

FIG. 2. Diffraction patterns of (a) the low-β hexagonal phase (β=3.5; Γ=36), (b) the lamellar complex obtained at intermediate values of β, and (c) the high-β hexagonal phase (β=9; Γ=36). The broader intermediate peak in (b) gives the average distance d_{DNA} between the DNA strands. β is the hexanol to CTAB molar ratio and Γ is the CTAB to DNA weight ratio.

similar in the positions of the peaks and their relative intensities, indicating that they arise from the same structure. Further all peaks have similar profiles [Fig. 2(a)]. The three reflections in each pattern can be indexed as (1 0), (1 1), and (2 0) on a 2D hexagonal lattice. The lattice parameter a is typically around 5.5 nm and decreases slightly with increasing hexanol and DNA concentrations.

For $5 < \beta < 8.5$ the diffraction patterns have two peaks with their q values in the ratio 1:2 and a third intermediate one. The intermediate peak is clearly broader than the other two [Fig. 2(b)], indicating a much shorter correlation length. The first two peaks can be assigned to a lamellar structure with a periodicity of about 4.9 nm, which is comparable to the sum of the bilayer thickness and the diameter of a hydrated DNA. Hence the structure formed by these complexes is similar to the lamellar structure observed earlier in some lipid/surfactant-DNA complexes [Fig. 1(a)], with the broader peak arising from the average separation between the DNA strands sandwiched between the lipid bilayers [1,4]. The formation of a lamellar phase is also consistent with the phase behavior of the CTAB-hexanol-water system, where the addition of hexanol is known to transform the cylindrical CTAB micelles into bilayers [11]. The positions of the first two peaks do not change significantly over the range of hexanol and DNA concentrations where such a pattern is found. On the other hand, the position of the intermediate peak shifts to larger angles with increasing DNA concentration near the isoelectric point, thus showing a decrease of the average in-plane DNA-DNA separation (Fig. 3).

Yet another structure is obtained when the hexanol content is further increased ($\beta > 8.5$) at low DNA concentrations ($\Gamma > \Gamma_{iso}$). It consists of a strong peak at q=1.44 nm^{-1} and a very weak peak at q=3.79 nm^{-1} [Fig. 2(c)]. These q-values are in the ratio $1:\sqrt{7}$, which can be indexed as the (1 0) and

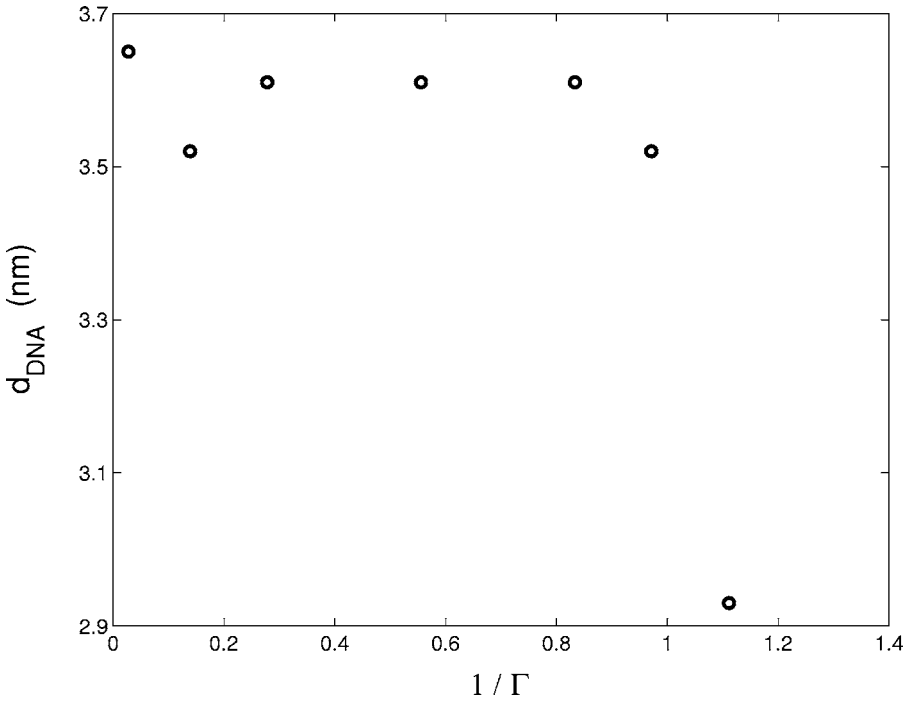

FIG. 3. Variation of the average in-plane distance between DNA strands with DNA concentration in the lamellar complex. Note the abrupt change in d_{DNA} near Γ_{iso}(=1.1). Typical error in d_{DNA} is ±0.05 nm. β=8.

(2 1) reflections from a two-dimensional hexagonal lattice with a lattice parameter a=4.36 nm. [An extremely weak (2 0) peak was seen after a very long exposure (≈5 h) using a laboratory source with a fairly large beam (≈2×2 mm).] Interestingly, these complexes precipitate out of the solution on formation, unlike the other two types which remain well dispersed in the aqueous solution. This behavior suggests that these complexes are hydrophobic. As discussed in Ref. [13], this structure transforms into the lamellar complex at higher DNA concentrations, due to the higher packing fraction of DNA possible in the latter structure.

The diffraction data, described above, clearly show the existence of three types of structures of DNA-CTAB-hexanol complexes, depending on the hexanol concentration. The structure occurring at intermediate hexanol concentrations can be identified as lamellar and its basic structural features can be deduced from the diffraction data. Unfortunately this is not the case with the other two structures. The diffraction patterns of the structure obtained at low hexanol content ($\beta < 5$) are very similar to that of CTAB-DNA complexes, both in the positions of the peaks and their relative intensities. Since CTAB forms cylindrical micelles, a very plausible structure of its complex with DNA is the intercalated hexagonal structure (H_I) shown in Fig. 1(c). Similarity of the diffraction patterns suggests that the hexagonal complex obtained at low values of β also has the same structure.

At high hexanol content an inverted hexagonal structure (H_{II}) similar to that seen in lipid-DNA systems may be proposed [Fig. 1(b)]. The observed hydrophobic nature of the complex is consistent with such a structure. Electrostatics would favor this structure over the others, since the greater proximity of the surfactant ions to the phosphate groups of the DNA leads to a more efficient neutralization in this geometry. However, the spontaneous curvature of the micelles and the bending rigidity of the bilayers would prevent its formation at lower hexanol concentrations. Inclusion of hexanol in the bilayer is known to reduce its bending rigidity drastically [12], and thus decreases the energy cost to wrap a surfactant monolayer around the DNA strands. Cosurfactants like hexanol can be incorporated both at the surfactant-water interface as well as in the hydrocarbon core of the micelles. Hence the frustration energy of the chains, at the interstitial regions where the three lipid-coated DNA strands meet, can also be reduced in the presence of hexanol [15]. These arguments suggest an inverted hexagonal structure of the complexes at high hexanol concentrations.

A. Modeling the structures

We have carried out a detailed analysis of the diffraction data in order to substantiate the structures of the two nonlamellar complexes proposed above. Since all the diffraction patterns contain only a few reflections, it is not possible to obtain electron density maps of sufficient resolution to unambiguously establish the structures. We have, therefore, modeled the two-dimensional electron densities of the two hexagonal structures and compared the calculated relative intensities with those observed. These models are taken to contain only a few adjustable parameters, as the diffraction data are limited.

The electron density $\rho_c(\vec{r})$ of these structures can be written as the convolution of a lattice function $\rho_l(\vec{r})$, which describes the two-dimensional hexagonal lattice, and the basis function $\rho(\vec{r})$, which describes the repeating motif within each unit cell of the lattice [16], i.e.,

$$\rho_c(\vec{r}) = \rho_l(\vec{r}) \otimes \rho(\vec{r}). \quad (1)$$

Fourier transforming this relation, we get

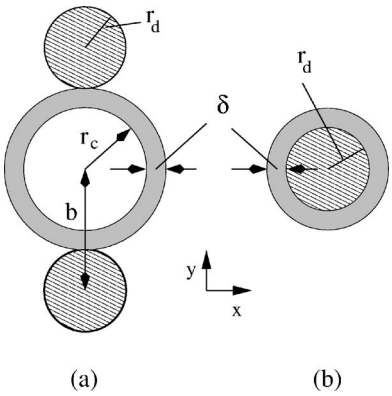

FIG. 4. The electron density models used in the calculation of the diffraction data. (a) H_I (b) H_{II}. The shaded disk represents the DNA strand and the annular rings the head-group region. The disk of radius r_c is the hydrocarbon region of the micelle. In the H_I structure the micelles and DNA strands are surrounded by water, whose electron density is, therefore, taken as the reference value. In the H_{II} structure water is intercalated with the DNA strands in the central pores of the inverted cylindrical micelles. In this case the reference value of the electron density is that of the background hydrocarbon region, which is, therefore, not shown in (b).

$$F(\vec{q}) = f_l(\vec{q}) \times f(\vec{q}), \tag{2}$$

where f_l and f are Fourier transforms of ρ_l and ρ, respectively.

The intensity of the scattered radiation, relative to that scattered by a single electron, is given by

$$I(\vec{q}) = |F(\vec{q})|^2. \tag{3}$$

In the H_I structure each unit cell contains one cylindrical micelle and two DNA strands [Fig. 1(c)]. Hexanol is incorporated in the micelles and the region between the micelles and DNA strands is occupied by water. There is some freedom in choosing this motif, since the positions of the DNA strands surrounding each micelle are related by unit cell translation vectors. We choose the symmetric motif shown in Fig. 4(a) for simplicity. In the H_{II} structure the motif consists of a hydrated DNA strand surround by an inverted cylindrical micelle [Figs. 1(b) and 4(b)]. In this case the central pore of each inverted micelle contains water along with a DNA strand, and hexanol molecules are incoporated in the micelles as in the former structure.

The hydrocarbon core of the cylindrical micelles is modeled as a circular disk of radius r_c with uniform electron density ρ_c, and the head group region as an annular ring of thickness δ with an electron density ρ_h (Fig. 4). The DNA are modeled as disks of radius r_d with a uniform electron density ρ_d. r_d is taken to be the radius of DNA with a hydration shell (1.25 nm). Values of ρ_c and the water electron density ρ_w were taken from the literature to be 280 and 332 e/nm^3, respectively [17]. The electron density of the head-group region ρ_h of a CTAB micelle is around 380 e/nm^3, due to the presence of a large number of Br^- counterions condensed on the micelle [18]. On complexation with DNA a fraction of these counterions will be released into the solution. From the area per charge of the DNA and CTAB micelles ($\sim$1.4 and $\sim$0.6 nm^2, respectively), we find that only about half of the counterions would be released even if all the charges on DNA are neutralized by the CTA^+ ions. Therefore, we would expect the value of ρ_h to decrease on complexation, although it would remain much higher than ρ_c. The electron density of hexanol, calculated from its density and molecular weight, is 280 e/nm^3, which is the same as that of the hydrocarbon region. Hence the inclusion of hexanol in the hydrocarbon region should not change ρ_c. On the other hand, incorporation of hexanol in the head-group region will increase the average separation between the electron-rich headgroups, and hence will result in a lower value of ρ_h. Therefore, we take ρ_h to be an adjustable parameter in the model. The other adjustable parameter is δ, which takes into account possible changes in the micellar size on complexation. Since DNA does not fill the cylindrical region of radius r_d, ρ_d has contributions from the water molecules present in this region, as well as from the atoms of the DNA itself. The contribution of DNA to ρ_d can be determined from its chemical structure, and is found to be 193 e/nm^3. The effective radius of a DNA strand, estimated from its molecular volume and contour length, is 0.77 nm [1]. The rest of the volume in the cylindrical region of radius r_d is occupied by intercalated water molecules, whose contribution to ρ_d can be estimated from its molar volume and electron density. This contribution turns out to be 207 e/nm^3, and hence $\rho_d \approx 400$ e/nm^3. If the contribution from the Na counter ions is also included, ρ_d goes up by about 10 e/nm^3. We have not taken this into account, since most of the counter ions are expected to be released from DNA on formation of the complex with CTAB.

1. The H_I structure

As the micelles and DNA strands are expected to be close packed in the H_I structure, the micellar size is related to lattice parameter a and r_d, by the relation, $r_c+\delta+r_d=a/\sqrt{3}$. Therefore, r_c and δ are not independent in this case. The value of $r_c+\delta$ obtained from this relation ($\sim$2 nm) is slightly lower than that reported in the literature ($\sim$2.2 nm) [18]. This difference might indicate a reduction in the micellar size on complexation, as found in other surfactant-polymer systems [19]. On the other hand, it might also, at least partially, be an artifact of approximating the DNA strands as cylinders. Each unit cell in the intercalated phase contains a cylindrical micelle and two DNA strands [Fig. 4(a)]. The electron density of this unit can be written as the convolution of the electron density of a DNA cylinder $\rho_{dna}(r)$ with delta functions representing their positions, plus the electron density of the micelle,

$$\rho^{H_I}(\vec{r}) = \rho_{dna}(r) \otimes \delta(r-b)\{\delta(\theta-\pi/2) + \delta(\theta+\pi/2)\} + \rho_m(r), \tag{4}$$

where θ is the angle between $\vec{r}$ and the x axis and $b(=r_c+\delta+r_d)$ the separation between the centers of the DNA strand and the micelle. $\rho_m(r)$ is the electron density of a CTAB micelle, given by

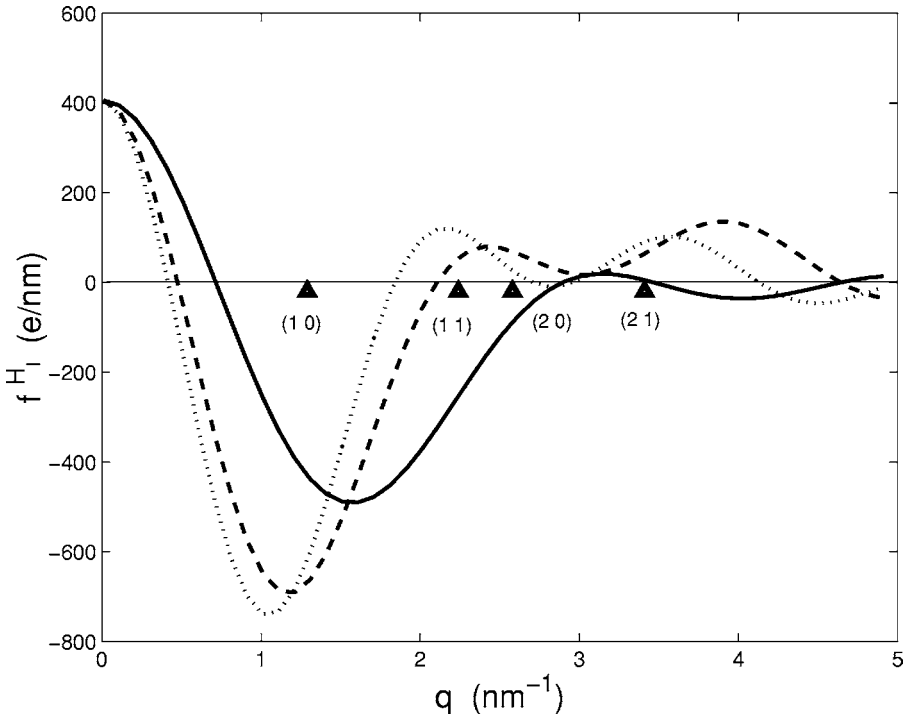

FIG. 5. Variation of the form factor of the H_I structure along $\hat{q}_{10}$ (solid line); $\hat{q}_{11}$ (dotted line); and $\hat{q}_{21}$ (dashed line) for $a=5.6$ nm, $\rho_h=340$ e/nm^3, and $\delta=0.6$ nm, corresponding to the data given in Table I for $\beta=0$. Values of the remaining parameters are $r_d=1.25$ nm, $\rho_d=400$ e/nm^3, $\rho_c=280$ e/nm^3, and $\rho_w=332$ e/nm^3. The positions of the peaks are indicated by the arrowheads.

$$\rho_m(r) = \rho_c - \rho_w,\ r < r_c$$
$$= \rho_h - \rho_w,\ r_c < r < r_c + \delta$$
$$= 0,\ r > r_c + \delta. \quad (5)$$

ρ_{dna} is taken as

$$\rho_{dna}(r) = \rho_d - \rho_w,\ r < r_d$$
$$= 0,\ r > r_d. \quad (6)$$

Fourier transforming $\rho^{H_I}(\vec{r})$ using the above expressions, we get the form factor of this structure

$$f^{H_I}(q,\phi) = 4\pi \cos(qb \sin\phi)(\rho_d - \rho_w) r_d J_1(qr_d)/q + f_m(q), \quad (7)$$

where ϕ is the angle made by the reciprocal lattice vector $\vec{q}$ with the x axis and $J_1(x)$ the Bessel function of order 1. $f_m(q)$ is the Fourier transform of $\rho_m(r)$, given by

$$f_m(q) = 2\pi(\rho_h - \rho_w) r_h J_1(qr_h)/q - 2\pi(\rho_h - \rho_c) r_c J_1(qr_c)/q, \quad (8)$$

where $r_h = r_c + \delta$. The variation of f^{H_I} along $\hat{q}_{10}$, $\hat{q}_{11}$, and $\hat{q}_{21}$ directions are shown in Figs. 5 and 6 corresponding to data

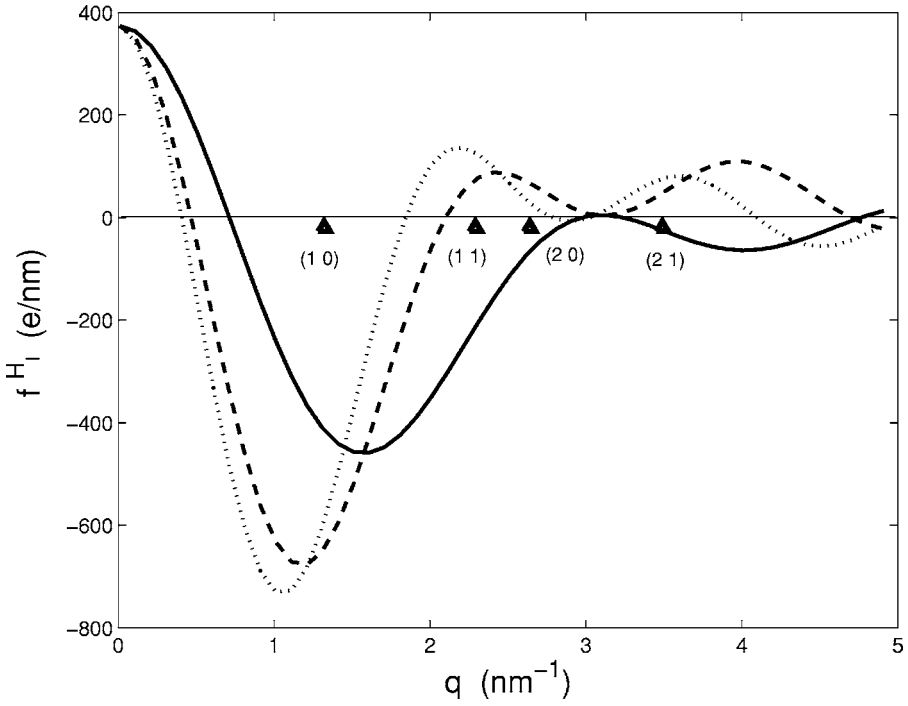

FIG. 6. Variation of the form factor of the H_I structure along $\hat{q}_{10}$ (solid line); $\hat{q}_{11}$ (dotted line); and $\hat{q}_{21}$ (dashed line) for $a=5.5$ nm, $\rho_h=325$ e/nm^3, and $\delta=0.7$ nm, corresponding to the data given in Table I for $\beta=3.5$. Values of the remaining parameters are the same as those given in the caption of Fig. 5. The positions of the peaks are indicated by the arrowheads.

TABLE I. Observed relative intensities (I_o) of the peaks in the diffraction pattern of DNA-CTAB complexes at three compositions, and those calculated from the H_I (I_{H_I}) and H_{II} ($I_{H_{II}}$) models. The best fit values of ρ_h and δ for the two models are also given below the respective intensity values. β is the hexanol to CTAB molar ratio and Γ is the CTAB to DNA weight ratio.

β=0, Γ=7.2					β=3.5, Γ=36					β=9.0, Γ=36				
h	k	I_o	I_{H_I}	$I_{H_{II}}$	h	k	I_o	I_{H_I}	$I_{H_{II}}$	h	k	I_o	I_{H_I}	$I_{H_{II}}$
1	0	100	100	100	1	0	100	100	100	1	0	100	100	100
1	1	7.0	7.2	6.9	1	1	9.2	9.4	9.2	1	1	-	2.7	0.4
2	0	1.3	4.2	1.4	2	0	2.3	2.6	1.9	2	0	-	2.4	0.4
2	1	-	2.2	0.4	2	1	-	1.3	0.9	2	1	0.3	2.7	0.7
ρ_h (e/nm^3)			340	297				325	290				340	315
δ (nm)			0.6	1.0				0.7	1.0				0.5	0.75

given in Table I for β=0 and 3.5, respectively.

2. The H_{II} structure

The r_c parameter does not enter the H_{II} model, since the hydrocarbon chains just provide a background of uniform electron density ρ_c. The repeating basis in the H_{II} structure is the DNA strand surrounded by an annular ring occupied by the surfactant head groups [Fig. 4(b)]. Its electron density can be written as

$$\begin{aligned}\rho^{H_{II}}(r) &= \rho_d - \rho_c,\ r < r_d \\ &= \rho_h - \rho_c,\ r_d < r < r_d + \delta \\ &= 0,\ r > r_d + \delta. \end{aligned} \tag{9}$$

Fourier transforming this expression, we get

$$f^{H_{II}}(q) = 2\pi(\rho_h - \rho_c)(r_t)J_1(qr_t)/q + 2\pi(\rho_d - \rho_h)r_d J_1(qr_d)/q, \tag{10}$$

where $r_t = r_d + \delta$. $f^{H_{II}}$ is shown in Fig. 7. Its first zero occurs at $q \sim 2.6$ nm^{-1}, beyond which its magnitude is negligible. Therefore, all the higher order reflections from this structure have to be very weak.

B. Model results

We have obtained the best fits of these two models to the diffraction data from the complexes at three different compositions. The observed intensities were multiplied by the square of the corresponding q values to take into account the unoriented nature of the samples. The intensity of the (2 1) reflection was also reduced by a factor of 2, since it has a multiplicity factor of 12, which is twice that of the (1 0),

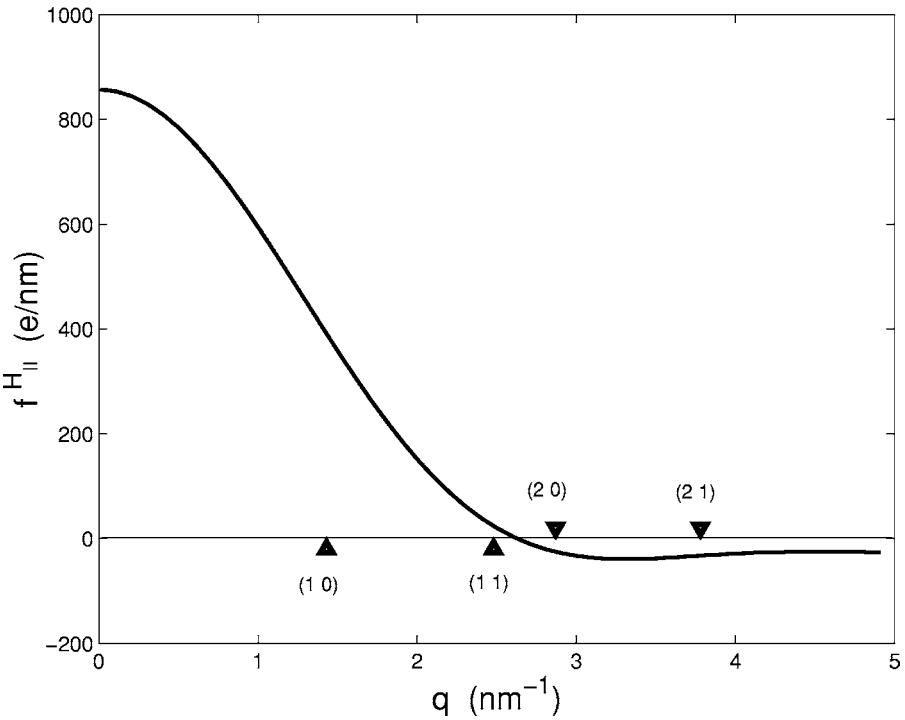

FIG. 7. Form factor of the H_{II} structure for ρ_h=315 e/nm^3, and δ=0.75 nm, corresponding to the data given in Table I for β=9. The rest of the parameters have the values given in the caption of Fig. 5. The positions of the peaks are indicated by the arrowheads.

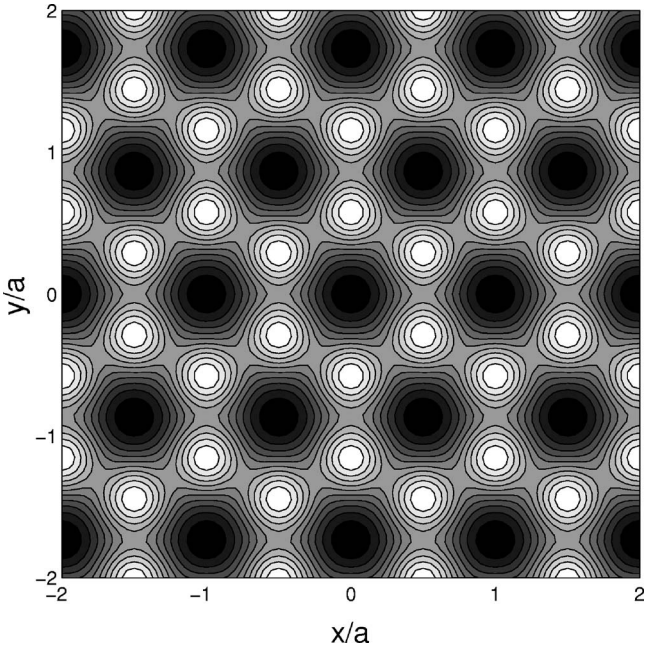

FIG. 8. Electron density map of the H^I phase corresponding to the data given in Table I for $\beta=0$, calculated using the phases obtained from the modeling procedure (Fig. 5). The electron density is higher in the lighter regions.

(1 1), and (2 0) reflections. As mentioned earlier, there are only two adjustable parameters in the two models, namely, the electron density of the head-group region ρ_h, and its thickness δ. The fits were obtained by constraining ρ_h between 280 and 400 e/nm^3 and δ between 0.3 and 1 nm. All the values of these parameters, reported in the literature for similar systems, are found to fall well within these ranges. Both in the hexanol-free complex and in the one with $\beta=3.5$, the (1 0), (1 1), and (2 0) reflections are observed, with $I_{10}>I_{11}>I_{20}$. As can be seen from Table I the H_I model is able to reproduce the sequence of observed intensities. This feature is not specific to the best fit values of ρ_h and δ, but is obtained for a wide range of their values. The values of these parameters obtained from this model are also comparable with those reported in the literature [20]. The lower value of ρ_h obtained at higher β (see Table I) is expected, since the incorporation of hexanol increases the average separation between the headgroups.

The form factor shown in Fig. 5 corresponds to the data given in Table I for $\beta=0$. The values of q corresponding to the (1 0), (1 1), and (2 0) reflections (1.29, 2.24, and 2.58 nm^{-1}, respectively) are well away from the corresponding zeros of the form factor and, therefore, their intensities are high enough to be observed. The form factor shown in Fig. 6 corresponds to the data given in Table I for $\beta=3.5$. In this case also the values of q corresponding to the (1 0), (1 1), and (2 0) reflections (1.32, 2.29, and 2.64 nm^{-1}, respectively) are well away from the corresponding zeros of the form factor.

Although the H_{II} model is also able to give good fits to the data at $\beta=0$ and 3.5, the resulting values of the material parameters are unrealistic. The value of ρ_h is too low and is almost comparable to ρ_c. Further, the value of δ obtained is set by the upper limit of the range over which it is constrained to vary; a better fit is obtained if it is allowed to take even larger values. Thus diffraction data of the low-β hexagonal complex is consistent only with the H_I structure, and the H_{II} structure can be ruled out.

In the case of the third complex ($\beta=9$, $\Gamma=36$) the (1 1) and (2 0) reflections are not seen, but a weak (2 1) reflection is present. This feature cannot be reproduced by the H_I model for any values of ρ_h and δ. The best it can do is to give similar intensities for these three reflections (Table I), but for a rather high value of ρ_h. As mentioned earlier, we would expect ρ_h to decrease with increasing β, and hence the value of 340 e/nm^3, which is equal to that obtained at $\beta=0$, is unreasonable. In contrast, the H_{II} model can give a stronger (2 1) reflection compared to (1 1) and (2 0) for wide range of values of ρ_h and δ. The best fit value of ρ_h (315 e/nm^3) is also understandable in light of the high concentration of hexanol. Note also that the best fit is obtained for a value of δ well within the range considered. Thus the diffraction pattern of this complex is consistent only with the H_{II} structure. The form factor of this structure shown in Fig. 7 corresponds to the data of Table I. The calculated positions of the (1 1) and (2 0) reflections in this case are 2.48 and 2.87 nm^{-1}, respectively. These lie very close and on either side of the first zero of the form factor, resulting in their negligible intensities. The (1 0) reflection at 1.43 nm^{-1} is very intense, but the (2 1) reflection at 3.78 nm^{-1} is very weak, since the form factor has a very small magnitude in this q-range.

Figure 8 presents the electron density map of the H_I phase calculated from the data for $\beta=0$ in Table I, using the phases obtained from Fig. 5. It clearly shows electron-rich patches intercalated between electron-poor regions. The former can be identified as the DNA strands and the latter as the CTAB micelles. The good quality of the map, where the micelles, DNA, and water regions are well demarcated, further supports the intercalated structure of the complexes obtained at low hexanol content.

IV. CONCLUSION

We have analyzed the diffraction patterns of CTAB-DNA-hexanol complexes at different hexanol concentrations. The complexes form hexagonal structures both at very high as well as at low hexanol concentrations. The two possible structures of these complexes, namely the intercalated and inverted hexagonal, were modeled and the calculated intensities of the diffraction peaks compared with the observed ones. The diffraction data at low hexanol content are found to be consistent only with an intercalated hexagonal structure, whereas those at high hexanol concentrations are compatible with only the inverted hexagonal structure.

[1] J. O. Raedler, I. Koltover, T. Salditt, and C. R. Safinya, Science **275**, 810 (1997).
[2] I. Koltover, T. Salditt, J. O. Raedler, and C. R. Safinya, Science **281**, 78 (1998).
[3] R. Ghirlando, E. J. Wachtel, T. Arad, and A. Minsky, Biochemistry **31**, 7110 (1992).
[4] R. Krishnaswamy, P. Mitra, V. A. Raghunathan, and A. K. Sood, Europhys. Lett. **62**, 357 (2003).
[5] R. Bruinsma, Eur. Phys. J. B **4**, 75 (1998).
[6] D. Harries, S. May, W. M. Gelbart, and A. Ben-Shaul, Biophys. J. **75**, 159 (1998).
[7] K. Wagner, D. Harries, S. May, V. Kahl, J. O. Raedler, and A. Ben-Shaul, Langmuir **16**, 303 (2000).
[8] D. Sennato, F. Bordi, and C. Cametti, Europhys. Lett. **68**, 296 (2004); T. T. Nguyen and B. I. Shklovskii, Rev. Mod. Phys. **74**, 329 (2002).
[9] T. Salditt, I. Koltover, J. O. Rädler, and C. R. Safinya, Phys. Rev. E **58**, 889 (1998).
[10] R. Krishnaswamy, V. A. Raghunathan, and A. K. Sood, Pramana, J. Phys. **61**, 447 (2003).
[11] P. Ekwall, L. Mandell, and K. Fontell, J. Colloid Interface Sci. **29**, 639 (1969).
[12] C. R. Safinya, E. B. Sirota, D. Roux, and G. S. Smith, Phys. Rev. Lett. **62**, 1134 (1989).
[13] R. Krishnaswamy, V. A. Raghunathan, and A. K. Sood, Phys. Rev. E **69**, 031905 (2004).
[14] H. Amenitsch, S. Bernstorff, M. Kriechbaum, D. Lombardo, H. Mio, M. Rappolt, and P. Laggner, J. Appl. Crystallogr. **30**, 872 (1997).
[15] S. May and A. Ben-Shaul, Biophys. J. **73**, 2427 (1997).
[16] See, for example, D. Sherwood, *Crystals, X-rays and Proteins* (Longman, London, 1976).
[17] B. Cabane, in *Surfactant Solutions: New Methods of Investigation*, edited by R. Zana (Marcel Dekker, New York, 1987).
[18] F. Husson, H. Mustacchi, and V. Luzzati, Acta Crystallogr. **13**, 668 (1960).
[19] P. Ilekti, L. Piculell, F. Tournilhac, and B. Cabane, J. Phys. Chem. B **102**, 344 (1998).
[20] F. Reiss-Husson and V. Luzzati, J. Phys. Chem. **68**, 3504 (1964).